

High-throughput computation and structure prototype analysis for two-dimensional ferromagnetic materials

Zhen-Xiong Shen^{1,2}, Chuanxun Su^{1,2,*}, and Lixin He^{1,2,**}

¹Key Laboratory of Quantum Information, University of Science and Technology of China, Hefei, 230026, China

²Synergetic Innovation Center of Quantum Information and Quantum Physics, University of Science and Technology of China, Hefei, 230026, China

*sucx@ustc.edu.cn

**helx@ustc.edu.cn

ABSTRACT

We perform high-throughput first-principles computations to search the high Curie temperature (T_C) two-dimensional ferromagnetic (2DFM) materials. We identify 79 2DFM materials and calculate their T_C , in which Co_2F_2 has the highest $T_C=541\text{K}$, well above the room temperature. The 79 2DFM materials are classified into different structural prototypes according to their structural similarity. We perform sure independence screening and sparsifying operator (SISSO) analysis to explore the relation between T_C and the material structures. The results suggest that the 2DFM materials with shorter distance between the magnetic atoms, larger local magnetic moments and more neighboring magnetic atoms are more likely to have higher T_C .

Introduction

Long-range magnetic order is suppressed in two-dimensional (2D) isotropic systems at finite temperatures due to thermal fluctuations, according to the Mermin-Wagner theorem¹. Therefore, recent discoveries of ferromagnetism in 2D materials, e.g., CrI_3 ^{2,3}, $\text{Cr}_2\text{Ge}_2\text{Te}_6$ ⁴, Fe_3GeTe_2 ^{5,6}, and Fe_4GeTe_2 ⁷ have attracted broad attention. The 2D ferromagnetic (2DFM) materials possess some fascinating in many aspects^{6,8,9}, which also have great potential in device applications, such as 2D spintronics¹⁰⁻¹⁴.

However, only very few 2DFM materials have been experimentally synthesized so far, and the Curie temperatures (T_C s) of these 2DFM materials are fairly low. The searching for 2DFM materials with high T_C via first-principles calculations attracts more and more attention. Mounet *et al* applied density functional theory (DFT) calculations to search for easily exfoliable magnetic compounds¹⁵, and they revealed a wealth of 2D magnetic systems including 37 ferromagnets. Zhu *et al* found 15 2DFM materials¹⁶. Especially, Cr_3Te_4 was predicted to have an extremely high $T_C=2057$ K. Torelli *et al* discovered 85 2DFM materials by high-throughput computation¹⁷. Kabiraj *et al.* found 26 2DFM materials with T_C higher than 400 K from high-throughput scanning of 786 materials¹⁸.

In this work, we carry out a comprehensive high-throughput computational study to calculate the T_C s of 2DFM materials. The magnetic exchange interactions are calculated via a first-principles linear response theory^{19–22}. We simulate the magnetic phase diagrams and evaluate the T_C by a replica-exchange Monte Carlo simulation²³. We have identified 79 2DFM materials. We benchmark the calculated T_C s with those of experimental synthesized materials, and also with the corresponding bulk materials. The results suggest that the results are highly reliable. The compound with the highest T_C we predicted is Co_2F_2 , which has $T_C=541\text{K}$. The 79 2DFM materials are classified into different structural prototypes according to their structural similarity. We perform sure independence screening and sparsifying operator (SISSO) analysis^{24,25} to explore the relation between T_C and the material structures. The results suggest that the 2DFM materials with shorter distance between the magnetic atoms, larger local magnetic moments and more neighboring magnetic atoms are more likely to have higher T_C .

Results

Two-dimensional magnetic atomic structural prototype

We select 198 2D magnetic materials which have high dynamical and thermodynamic stability in the Computational 2D Materials Database (C2DB)^{26–28}. We also calculate 37 compounds from Ref.¹⁵, and 8 compounds from Ref.¹⁶. In addition to these materials, we also include several experimentally synthesized structures such as CrI_3 ^{2,3}, $\text{Cr}_2\text{Ge}_2\text{Te}_6$ ⁴, Fe_3GeTe_2 ^{5,6}, and Fe_4GeTe_2 ⁷. The workflow and calculation details are presented in Sec.. There are some 2D materials that show complicated magnetic ground states, which will be interesting for further studies. In this work, we focus on the FM materials, which have great potential in device applications.

We find 79 2D magnetic materials that have robust FM ground states. We analyze the structural characters of these 2DFM materials. For simplicity, we first consider only the magnetic atoms in the unit cell. The 79 2DFM structures can be divided into 11 categories according to the structural similarity of the magnetic atoms. The prototypical structures of the 11 categories are

shown in Fig. 1. In Table 1, we list the chemical formula of materials as well as their space groups contained in each category. For convenience, we use “Chemical formula-Magnetic atom” to name the magnetic atomic structure prototypes. There are 6 categories, including $Zr_2I_2S_2$ -Zr, EuOI-Eu, $V_3N_2O_2$ -V, Cr_3Te_4 -Cr, Fe_3GeTe_2 -Fe, and Fe_4GeTe_2 -Fe that each contains only one material. The remaining 73 materials are divided into five categories. Note that all the 2DFM materials studied in this work contain only one type of magnetic atom in each structure. The decoration of nonmagnetic atoms can change the structure dramatically. For example, if the nonmagnetic atoms are taken into account, the 29 original structures of the FeI_2 -Fe prototype can be further divided into 4 different structures according to their structural similarity.

Among these 79 materials, some have multiple layers of magnetic atoms. Note that the layers we refer to here are those between the layers, the ions form strong chemical bonds, instead of weak van de Waals bonds. Among the 11 prototype categories, 4 have a single layer of magnetic atoms, 3 have double magnetic layers, 3 have triple magnetic layers, and 1 has quadruple layers. Obviously, the structures of different magnetic layers differ greatly.

The category of FeI_2 -Fe contains 29 2DFM materials, which is the most popular magnetic atomic structure prototype, and the magnetic atoms in this structure prototype reside on the same plane. The original structures have 3 different space groups $P-6m2$, $P-3m1$, and $P3m1$. The composition types of these structures are AB_2 and ABC. The CrI_3 -Cr prototype with only one layer of magnetic atoms contains 14 2DFM materials which possess the $P-62m$ and $P-31m$ space groups, and adopt AB_3 and ABC_3 composition types. This category includes the famous CrI_3 compound, which has been experimentally synthesized², and investigated intensively.

For VO_2 -V prototype, the magnetic atoms also reside in one plane, and there are $P4/nmm$, $P-4m2$, and $P4/mmm$, three different space groups for the original structures. The composition types are AB and AB_2 . The Co_2F_2 -Co prototype, which has double magnetic atom layers, has 6 2DFM materials and contains AB and ABC two different composition types. Their space groups are all $P-3m1$. There are 9 2DFM materials with ABC composition type and $Pmmn$ space group belongs to $Cr_2I_2S_2$ -Cr prototype.

Curie temperatures

The calculated T_C s for the 79 2DFM materials are also listed in Table 1. Since T_C s of some of the 2DFM materials have been measured experimentally, we first compare the calculated T_C s to the experimental values for these materials. The calculated T_C of monolayer CrI_3 is 26 K, which is slightly lower than 45 K of the experimental value² and very close to the other theoretical calculation of 28 K¹⁷. The magnetic order at finite temperature can be stabilized when applying a small external magnetic field

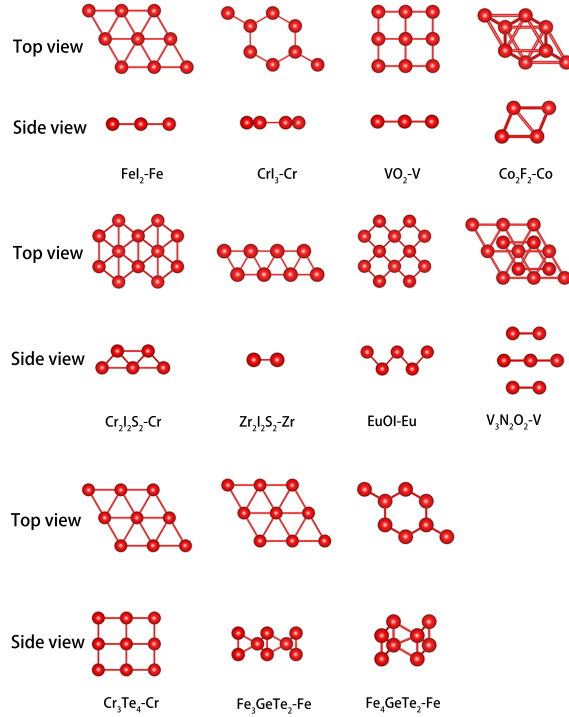


Figure 1. The structure prototypes of 2DFM materials with only magnetic atoms kept.

to $\text{Cr}_2\text{Ge}_2\text{Te}_6$ ⁴. The calculated T_C of $\text{Cr}_2\text{Ge}_2\text{Te}_6$ ⁴ is 11 K with 0.25 meV/Cr magnetic anisotropic energy is very close to the estimated experimental value, and is slightly lower than the theoretical estimation of 20 K in Ref.⁴. It is worth mentioning that the calculated T_C of Fe_3GeTe_2 is 158 K²⁹, which is close to the experimental value of 130 K⁵. Our calculated T_C of monolayer Fe_4GeTe_2 is about 207 K which is below 270 K of its bulk phase⁷. We also calculate the T_C of monolayer Cr_3Te_4 , and obtain $T_C=133$ K, which is also lower than the experimental $T_C=316$ K of the bulk material³⁰, as expected. Note that in Ref.¹⁶, the T_C of monolayer Cr_3Te_4 was severely overestimated to be 2057 K, much higher than the T_C of the bulk Cr_3Te_4 . All these results suggest that our calculated T_C s of the 2DFM materials are highly reliable. The exchange interactions calculated by the linear response theory are somehow smaller than those calculated by the energy mapping method¹⁶⁻¹⁸, and therefore the calculated T_C s are also lower.

The distributions of T_C s of the first five categories of 2DFM materials are shown in Fig. 2. The average T_C of the 73 materials is 71 K. The average T_C for $\text{FeI}_2\text{-Fe}$, $\text{CrI}_3\text{-Cr}$, $\text{VO}_2\text{-V}$, $\text{Co}_2\text{F}_2\text{-Co}$, and $\text{Cr}_2\text{I}_2\text{S}_2\text{-Cr}$ categories are 66 K, 38 K, 84 K, 132 K, and 88 K, respectively. The ratio of structures that have T_C higher than the average value (71 K) for the above categories are 34%, 0%, 60%, 33%, and 78%, respectively. The last 6 prototypes in TABLE 1 have only one 2DFM material in each category. Among them, the T_C s of $\text{V}_3\text{N}_2\text{O}_2$, Cr_3Te_4 , Fe_3GeTe_2 , and Fe_4GeTe_2 are 71 K, 133 K, 158 K, and 207 K, respectively.

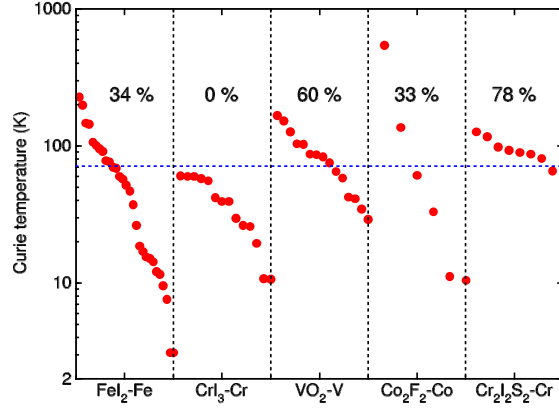


Figure 2. The distribution of T_C for 73 2DFM materials in different structure prototypes. The T_C s are arranged in descending order. Blue dot line marks the average T_C for the 73 structures. The percentages are the ratios of structures that have T_C above the average Curie temperature for each category.

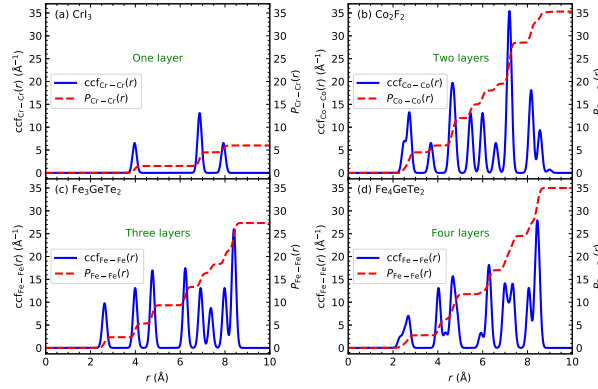


Figure 3. The $ccf_{ij}(r)$ and their integral $P_{ij}(r)$ for (a) CrI_3 , (b) Co_2F_2 , (c) Fe_3GeTe_2 , and (d) Fe_4GeTe_2 .

Among the 79 2DFM materials, Co_2F_2 has the highest $T_C=541$ K. The T_C s of the rest materials are all below room temperature, which is not very surprising. We find 3 materials whose T_C are higher than 200 K, and 4 materials, whose T_C are between 150 K and 200 K. There are 11 materials with T_C between 100 K and 150 K. These results suggest that the T_C s of 2DFM materials are relative low, compared to the 3D compounds, and finding room temperature 2DFM materials is quite difficult. The T_C s of previous calculations^{16,18} are generally higher than the ones in this work. Especially, in Ref.¹⁶, heuristic factors 0.2 - 0.4 are multiplied to obtain reasonable T_C s.

Discussion

Structure characteristics

It is important to understand the relation between the structure and T_C . We have checked that the cation-anion-cation angles of all the 79 2DFM materials are close to 90° , which obey the Goodenough-Kanamori rule^{31,32} for the FM exchange interactions.

For example, the bond angles of Cr-O-Cr for CrO₂ and Fe-Cl-Fe angle for FeCl₂ are 97.53° and 85.49° respectively.

Naively, one could expect that having more neighboring magnetic atoms may lead to higher T_C for a material. The coordination characterization function (CCF)³³ defined in Sec. can reflect the coordination character of the structure, and the abscissa of the peak of CCF corresponds to the length of a atomic pair. The integral of CCF,

$$P_{ij}(r) = \int_0^r \text{ccf}_{ij}(r') dr', \quad (1)$$

characterizes the average number of (magnetic) atomic pairs within a certain range r , where $\text{ccf}_{ij}(r')$ is the CCF for the i -th and j -th type of element of the structure.

The $\text{ccf}_{ij}(r)$ (red solid lines) and $P_{ij}(r)$ (blue dashed lines) of four representative structures, CrI₃, Co₂F₂, Fe₃GeTe₂, and Fe₄GeTe₂, from different structure prototypes are shown in Fig. 3. These structures have different numbers of magnetic atomic layers. CrI₃ has quite low T_C , which is about 26 K, whereas other components have much higher T_C . Especially, the T_C of Co₂F₂ is about 543 K, which is the highest among the 79 2DFM materials. Fe₃GeTe₂, and Fe₄GeTe₂ also have relative high T_C . By comparing the $\text{ccf}_{ij}(r)$ and $P_{ij}(r)$ of different structures, obviously CrI₃ has much less neighboring magnetic atoms within given the range than other three components, due to two reasons. The first factor that affect $\text{ccf}_{ij}(r)$ and $P_{ij}(r)$ is the length between the nearest magnetic atoms, d_{\min} . The smaller d_{\min} will increase the neighboring magnetic atoms, and it may also lead to larger exchange interactions between magnetic atoms, which therefore leads to higher T_C . The d_{\min} of Co₂F₂ is very small (~ 2.48 Å), due to the small radii of F atoms. The d_{\min} s of Fe₃GeTe₂ and Fe₄GeTe₂ are also quite small ~ 2.5 Å. In contrast, the d_{\min} of CrI₃ is about 3.97 Å, which is much larger than those of the other three compounds. The $\text{ccf}_{ij}(r)$ and $P_{ij}(r)$ are also related to the number of magnetic atomic layers for the materials. For example, CrI₃ has only a single layer of magnetic atoms, whereas Co₂F₂ has two magnetic layers and Fe₃GeTe₂, Fe₄GeTe₂ have 3 and 4 magnetic layers respectively, which therefore have more neighboring magnetic atoms. From Table I, one may find that the 2DFM materials with multiple magnetic atomic layers are more likely to have higher T_C . In fact, the T_C s of the most compounds of a single magnetic layer are relatively low, except CrO₂ and FeCl₂.

The magnetization intensity is often used to evaluate bulk magnetic materials. For 2DFM materials, we define the areal magnetic moment density to measure their macroscopic magnetization,

$$\mathbf{M}_{2D} = \frac{\mathbf{m}_{\text{cell}}}{s_{\text{cell}}}, \quad (2)$$

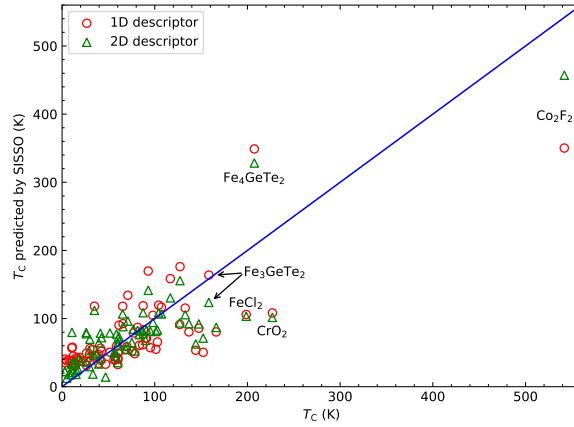


Figure 4. The T_C predicted by SISSO vs. the T_C calculated via the high-throughput first-principles calculations. The red circles are the results of 1D descriptor, whereas the green triangles are the results of 2D descriptor.

where \mathbf{m}_{cell} is the total magnetic moment of the unit cell, and s_{cell} is the area of the 2D unit cell. 2DFM materials with larger \mathbf{M}_{2D} have stronger magnetism and are more favorable for applications. Obviously, the 2DFM material with denser magnetic atomic mesh, multiple magnetic layers, and larger local magnetic moments would have larger \mathbf{M}_{2D} . For example, the \mathbf{M}_{2D} for Co_2F_2 , Fe_4GeTe_2 , and Fe_3GeTe_2 are 0.74, 0.59, and 0.33 $\mu_B/\text{\AA}^2$, respectively. They are much larger than that of CrI_3 0.15 $\mu_B/\text{\AA}^2$. This is because Co_2F_2 has two layers of magnetic atoms, which are densely packed. Fe_4GeTe_2 and Fe_3GeTe_2 have 4 and 3 layers of Fe atoms. In contrast, CrI_3 has only one layer of magnetic atoms, with relatively larger Cr-Cr pair lengths. Interestingly, Co_2F_2 possesses both the highest T_C and the highest \mathbf{M}_{2D} among the 79 2DFM materials, showing that it is a promising material.

SISSO analysis of Curie temperature

To dig out the factors that determine the T_C of the 2DFM materials, we resort to the recently developed SISSO method which may capture the underlying mechanisms of materials' properties using small data sets^{24,25}. We use three parameters to construct the model, including the magnetic moment (M in μ_B per spin), the minimum magnetic atomic distance (d_{min} , in \AA), and the integral of CCF (P) as typical features to predict the T_C of the above 2DFM materials. Among the three parameters, M is an important physical feature of the magnetic atoms, whereas d_{min} and P are used to characterize the structures of the magnetic atoms. The cutoff radius of $P_{ij}(r)$ is set to be 7.0 \AA to calculate the P of the above 79 magnetic atomic structures.

Figure 4 illustrates the T_C predicted by SISSO vs. the *ab initio* calculated T_C . The one dimensional (1D) descriptor²⁵ fitting

gives,

$$T_C = 27.88 + 110.03 \times \frac{M \times P}{d_{\min}^3}, \quad (3)$$

and 2D descriptor gives,

$$T_C = 139.33 + 0.0078 \times \frac{M^3 \times P^4}{d_{\min}^4} - 1.44 \times \frac{P^{\frac{1}{4}} \times d_{\min}^3}{M^{\frac{1}{2}}}. \quad (4)$$

The root mean square error (RMSE) for 2D descriptor is 38 K, which is somehow smaller than that of the 1D descriptor of 46 K. According to the results of SISSO, it is clear that T_C has a positive correlation with M and P , and negative correlation with d_{\min} , which is consistent with the analysis in the previous paragraphs.

The SISSO method correctly produces that Co_2F_2 has very high T_C , because Co_2F_2 meets all the above beneficial conditions for high T_C . The d_{\min} for Co_2F_2 is only 2.48 Å, and the next nearest neighbor is as short as 2.73 Å. The exchange interaction between the nearest neighbor Co-Co pairs in Co_2F_2 is calculated to be -35.43 meV, and the exchange interaction between the next nearest neighbor Co-Co pair is -15.28 meV. Furthermore, there are about 20 Co-Co pairs with a mutual distance smaller than 7.0 Å for each Co atom, as shown in Fig. 3(d). All these physical quantities suggest that it should have a high T_C .

On the other hand, the T_C s of the compounds in the CrI_3 -Cr structural prototype are quite low. For example, CrI_3 has a low T_C 26 K. It has only one magnetic atomic layer and for each Cr atom, there are only 5 Cr-Cr pairs within 7.0 Å. The d_{\min} is as large as 3.97 Å. The situations for other structures of CrI_3 -Cr structural prototype are similar.

However, the magnetic interactions have very complicated mechanisms, and the T_C s are determined by many factors. One would not expect that the simple SISSO models can predict very accurate T_C s for the 2DFM materials. For example, while the SISSO method predicts the T_C s of Fe_3GeTe_2 rather well, it somehow over estimates the T_C of Fe_4GeTe_2 . They also underestimate the T_C of FeCl_2 and CrO_2 . Nevertheless, it gives correct trends of T_C respect to the structure of the 2DFM materials, which may provide useful guidance to further searching of high T_C 2DFM materials.

Finally, we note that the PBE functional used in this work is suitable for large-scale, fast screening of the materials, but it is known to have some deficiencies. Once we find the promising candidate materials, we can use advanced techniques³⁴⁻³⁷ to obtain more accurate results for the electronic and magnetic structures. Furthermore, the 2D structures studied in this work are taken from existing databases. It is possible to investigate a wider range of 2D magnetic materials via crystal structure prediction methods.^{38,39}

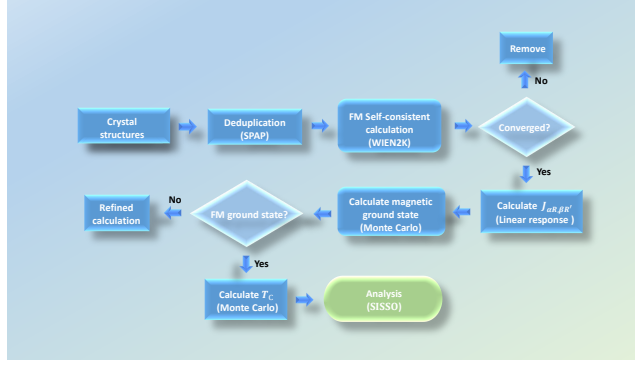


Figure 5. The workflow of the high-throughput computation of the 2D magnetic materials.

In this work, we carry out high-throughput first-principles computations to search for potential high T_C 2DFM materials. We identify 79 2D materials that have robust FM ground state and calculate their T_C s. Among the 79 2DFM materials, Co_2F_2 has the highest $T_C=541\text{K}$, well above room temperature. There are three 2D materials that also have relative high T_C , including CrO_2 (226 K), FeCl_2 (198 K), and Fe_4GeTe_2 (207 K). We perform SISSO method to analyze the relations between the T_C and the structure of the 2DFM materials. The results suggest that the 2DFM materials with smaller distance between the magnetic atoms d_{\min} , larger local magnetic moments and more neighboring magnetic atoms are more likely to have higher T_C . Our research is instructive to the discovery of new 2DFM materials with high T_C .

Methods

Workflow

The work flow of our high-throughput computations is illustrated in Fig. 5. This high-throughput computing process is highly automated and almost no empirical parameters are introduced. Once the basic 2D magnetic crystals are collected, we run the Structure Prototype Analysis Package (SPAP) code³³ to cluster structures according to structural similarity and label the structures with corresponding structure prototypes. We then perform self-consistent first-principle calculations, and some non-convergent structures will be removed at this step. The magnetic exchange interactions $J_{\alpha\mathbf{R},\beta\mathbf{R}'}$ are calculated by a linear response method^{21,22}. Based on the calculated magnetic exchange parameters, the magnetic ground state of the system is simulated by the Monte Carlo method at $T \approx 0$ K. If the ground state is ferromagnetic, the T_C will be calculated. We carry out further analysis based on these results.

Structure prototype analysis

The properties of the materials are determined by their constituting elements and the residing structure. A group of materials having similar structures tend to possess similar properties. In order to find out the relationship between the T_C (and other magnetic properties) of the 2DFM materials and their structures, we categorize the 2DFM materials according to their structural similarity. We use the SPAP code to classify these structures into corresponding structure prototypes, and details of the methods are given in Ref.³³. Different from the similarity comparisons of bulk crystal structures, which needs to normalize two structures to the same volumetric atom number density, for 2D materials, we need to construct an areal atom number density normalization coefficient,

$$c_{2D} = \sqrt{\frac{S_A N_B}{S_B N_A}}, \quad (5)$$

where S_A , S_B , N_A , and N_B denote the area of the 2D lattice of structure A and B , and the number of atoms in the 2D cell of structure A and B , respectively. We multiply the 3 lattice vectors of structure B by c_{2D} . Note that the fractional coordinates of the atoms of the structure B should be kept unchanged. The manipulated structure B is adjusted to the same areal atom number density with that of structure A . The normalization helps us to identity similar structures with different scales. We use the CCF³³ to measure the distance between normalized structures, which is defined as follows, for pairs of atomic types i and j ,

$$ccf_{ij}(r) = \left(1 - \frac{1}{2}\delta_{ij}\right) \frac{1}{N} \sum_{n_i} \sum_{n_j} f(r_{n_i n_j}) \sqrt{\frac{a_{pw}}{\pi}} e^{-a_{pw}(r - r_{n_i n_j})^2}, \quad (6)$$

where N is the total number of atoms in the cell. n_i runs over all atoms of the i -th type within the unit cell, whereas, n_j runs over all atoms of the j -th type within the extended cell. $f(r_{n_i n_j})$ is the weighting function for different interatomic distances, whereas $r_{n_i n_j}$ is the interatomic distance within the cutoff radius. a_{pw} (usually 60.0 \AA^{-2}) is a parameter that controls the width of the normalized Gaussian smearing function.

We assign similar structures with the same prototype name with the help of three norms: (i) the same composition type and total number of atoms in the conventional cell; (ii) equivalent three-dimensional crystal symmetry; and (iii) the distance between two structures being below a threshold. In this work, we take 0.075 as the threshold. After the structural classification by SPAP, the structures are rechecked visually to guarantee that similar structures are labeled with the same prototype name.

Density functional calculation

The structural, electronic, and magnetic properties of the 2D magnetic materials are studied via density functional theory (DFT) by the WIEN2K code, which is based on a full-potential linearized augmented plane wave method (FP-LAPW)⁴⁰. We adopt the Perdew-Burke-Ernzerhof (PBE) form generalized gradient approximation (GGA) of the exchange-correlation functional⁴¹. For all calculated materials, 1000 Brillouin k -points are used, and the number of k -points are automatically assigned according to the shape of the unit cell. The plane-wave cutoff $RK_{max} = 7$ is used.

Magnetic exchange interactions

In previous works^{16–18,42}, the magnetic exchange interactions are usually calculated via an energy mapping method, i.e., the total energies of different spin configurations are calculated, and the exchange interactions are fitted to the energies of different spin configurations. There are several disadvantages of this method. First, this method is not user-friendly for the high-throughput calculations, since the spin configurations have to be chosen by hand for each material, with caution. Different choices of the spin configurations may lead to large discrepancies in the results. This is because, for some spin configurations, the electrons are forced to occupy higher energy orbitals, and in these cases, the total energies can not be fitted very well by the Heisenberg model, because an additional electron band (the so-called Stoner) energies have to be considered. The exchange interactions calculated by the energy mapping method may thus be overestimated and this might be one of the reasons that some of the previous works significantly overestimated the T_C ¹⁶. Furthermore, for some materials, the long-range exchange interactions are important for T_C ¹⁸. To take account of the long-range magnetic interactions, very large supercells are required to obtain the exchange interactions.

In this work, we calculate the magnetic interactions via a first-principle linear-response approach^{21,22}, where the magnetic exchange interaction is calculated as:

$$J_{i\mathbf{R},j\mathbf{R}'} = \sum_{\mathbf{q}} \sum_{kmm'} \frac{f_{nk} - f_{n'\mathbf{k}+\mathbf{q}}}{\epsilon_{nk} - \epsilon_{n'\mathbf{k}+\mathbf{q}}} \langle \psi_{nk} | [\boldsymbol{\sigma} \times \mathbf{B}_i] | \psi_{n'\mathbf{k}+\mathbf{q}} \rangle \times \langle \psi_{n'\mathbf{k}+\mathbf{q}} | [\boldsymbol{\sigma} \times \mathbf{B}_j] | \psi_{nk} \rangle e^{i\mathbf{q} \cdot (\mathbf{R} - \mathbf{R}')}, \quad (7)$$

where, ϵ_{nk} is the one-electron band energy, $\boldsymbol{\sigma}$ are the Pauli matrices. ψ_{nk} is the Kohn-Sham wave function, \mathbf{B}_i is the local magnetic field, \mathbf{R} is the unit cell index, whereas i is the atom in the \mathbf{R} -th unit cell. This technique has been successfully applied to a wide variety of complex magnetic materials^{22,29,43–45}. Details about the method can be found in Ref.^{21,22}. In this work, we calculate all the eligible exchange interactions $J_{i\mathbf{R},j\mathbf{R}'}$, i.e., the exchange interactions between the i -th spin in the \mathbf{R} -th unit cell and the j -th spin in the \mathbf{R}' -th unit cell, within the range of $|\mathbf{R}'_{\alpha} - \mathbf{R}_{\alpha}| \leq 3$, where $\alpha = a, b, c$.

Replica-exchange Monte Carlo simulation

The magnetic phase diagrams and the T_C s are simulated via the following anisotropic Heisenberg-like Hamiltonian,

$$H = \sum_{i\mathbf{R},j\mathbf{R}'} J_{i\mathbf{R},j\mathbf{R}'} \mathbf{S}_{i\mathbf{R}} \cdot \mathbf{S}_{j\mathbf{R}'} + \sum_i A(S_i^z)^2, \quad (8)$$

where $\mathbf{S}_{i\mathbf{R}}$ is the i -th spin in the \mathbf{R} -th unit cell. The magnetic anisotropy energy A is important to stabilize the ferromagnetism in 2D. Because the magnetic anisotropy energy A is very sensitive to the calculation parameters, it is still quite difficult to obtain highly accurate and reliable values in the high-throughput DFT calculations. Fortunately, we find that T_C is not very sensitive to the value of A , as demonstrated in our previous works²⁹. For example, the T_C of CrI₃ with the magnetic anisotropic energy $A=0.25$ meV for each Cr ion is 26 K, whereas the T_C only increases to 30 K when $A=1.00$ meV is used. Therefore we set a reasonable value $A=0.25$ meV per spin for all materials, which is enough for our purpose. We simulate the above spin Hamiltonian via the replica-exchange Monte Carlo method^{23,46,47}, in which one simulates M replicas each at a different temperature T covering a range of interest, allowing configurational exchange between the replicas. The simulations are performed on a 36×36 lattice with periodic boundary conditions. We first perform the simulations at temperatures ranging from 5 to 640 K using 120 replicas. If no FM phase transition is found, we then perform simulation at temperatures ranging from 0.2 to 20 K. We discard the first 2×10^5 sweeps, when computing the equilibrium properties. Sample averages are accumulated over 2×10^5 sweeps.

SISSO analyses

SISSO is an approach for discovering descriptors for materials' properties, which can tackle huge and possibly strongly correlated feature spaces, and converges to the optimal solution from a combination of features relevant to the materials' target property. The outcome of SISSO is explicit, analytic functions consisted of basic physical quantities. A detailed description of the method can be found in Refs.^{24,25}. In this work, the SISSO code from github.com/rouyang2017/SISSO is used to perform the analyses.

DATA AVAILABILITY

All data generated and/or analyzed during this study are included in this article.

CODE AVAILABILITY

The SPAP code is available at <https://github.com/chuanxun/StructurePrototypeAnalysisPackage>. The homemade Monte Carlo simulation code is available upon request to He, Lixin (helx@ustc.edu.cn). The linear-response code to calculate the exchange interactions is available upon request to Wan, Xiangang (xgwan@nju.edu.cn).

Acknowledgements

We appreciate Prof. Wan, Xiangang for generously allowing us to use the linear-response code. This work was funded by the Chinese National Science Foundation Grant Number 12134012. The numerical calculations were done on the USTC HPC facilities.

AUTHOR CONTRIBUTIONS

Z. Shen and C. Su performed the calculations. All authors analyzed the results and wrote the manuscript. L. He conducted the project.

Competing interests:

The authors declare no competing interests.

References

1. Mermin, N. D. & Wagner, H. Absence of ferromagnetism or antiferromagnetism in one- or two-dimensional isotropic heisenberg models. *Phys. Rev. Lett.* **17**, 1133–1136 (1966).
2. Huang, B. *et al.* Layer-dependent ferromagnetism in a van der waals crystal down to the monolayer limit. *Nature* **546**, 270–273 (2017).
3. Thiel, L. *et al.* Probing magnetism in 2d materials at the nanoscale with single-spin microscopy. *Science* **364**, 973–976 (2019).
4. Gong, C. *et al.* Discovery of intrinsic ferromagnetism in two-dimensional van der waals crystals. *Nature* **546**, 265–269 (2017).
5. Fei, Z. Y. *et al.* Two-dimensional itinerant ferromagnetism in atomically thin fe_3gete_2 . *Nat. Mater.* **17**, 778–782 (2018).

6. Deng, Y. *et al.* Gate-tunable room-temperature ferromagnetism in two-dimensional Fe_3GeTe_2 . *Nature* **563**, 94–99 (2018).
7. Seo, J., Kim, D. Y., An, E. S., Kim, K. & Kim, J. S. Nearly room temperature ferromagnetism in a magnetic metal-rich van der Waals metal. *Sci. Adv.* **6**, eaay8912 (2020).
8. Gong, C. & Zhang, X. Two-dimensional magnetic crystals and emergent heterostructure devices. *Science* **363**, eaav4450 (2019).
9. Sun, Z. *et al.* Giant nonreciprocal second-harmonic generation from antiferromagnetic bilayer CrI_3 . *Nature* **572**, 497–501 (2019).
10. Wang, Z. *et al.* Very large tunneling magnetoresistance in layered magnetic semiconductor CrI_3 . *Nat. Commun.* **9**, 2516 (2018).
11. Song, T. *et al.* Giant tunneling magnetoresistance in spin-filter van der Waals heterostructures. *Science* **360**, 1214–1218 (2018).
12. Klein, D. R. *et al.* Probing magnetism in 2d van der Waals crystalline insulators via electron tunneling. *Science* **360**, 1218–1222 (2018).
13. Kim, H. H. *et al.* One million percent tunnel magnetoresistance in a magnetic van der Waals heterostructure. *Nano Lett.* **18**, 4885–4890 (2018).
14. Wang, Z. *et al.* Tunneling spin valves based on $\text{Fe}_3\text{GeTe}_2/\text{hBN}/\text{Fe}_3\text{GeTe}_2$ van der Waals heterostructures. *Nano Lett.* **18**, 4303–4308 (2018).
15. Mounet, N. *et al.* Two-dimensional materials from high-throughput computational exfoliation of experimentally known compounds. *Nat. Nanotechnol.* **13**, 246–252 (2018).
16. Zhu, Y., Kong, X., Rhone, T. D. & Guo, H. Systematic search for two-dimensional ferromagnetic materials. *Phys. Rev. Mater.* **2**, 81001 (2018).
17. Torelli, D., Moustafa, H., Jacobsen, K. & Olsen, T. High-throughput computational screening for two-dimensional magnetic materials based on experimental databases of three-dimensional compounds. *npj Comput. Mater.* **6**, 158 (2020).
18. Kabiraj, A., Kumar, M. & Mahapatra, S. High-throughput discovery of high Curie point two-dimensional ferromagnetic materials. *npj Comput. Mater.* **6**, 35 (2020).

19. Liechtenstein, A. I., Katsnelson, M. I., Antropov, V. P. & Gubanov, V. A. Local spin density functional approach to the theory of exchange interactions in ferromagnetic metals and alloys. *J. Magn. Magn. Mater.* **67**, 65–74 (1987).
20. Bruno, P. Exchange interaction parameters and adiabatic spin-wave spectra of ferromagnets: A “renormalized magnetic force theorem”. *Phys. Rev. Lett.* **90**, 087205 (2003).
21. Wan, X., Yin, Q. & Savrasov, S. Y. Calculation of magnetic exchange interactions in mott-hubbard systems. *Phys. Rev. Lett.* **97**, 266403 (2006).
22. Wan, X., Maier, T. & Savrasov, S. Y. Calculated magnetic exchange interactions in high-temperature superconductors. *Phys. Rev. B* **79**, 155114 (2009).
23. Cao, K., Guo, G.-C., Vanderbilt, D. & He, L. First-principles modeling of multiferroic rmn_2o_5 . *Phys. Rev. Lett.* **103**, 257201 (2009).
24. Fan, J. & Lv, J. Sure independence screening for ultrahigh dimensional feature space. *J. R. Statist. Soc. B* **70**, 849–911 (2008).
25. Ouyang, R., Curtarolo, S., Ahmetcik, E., Scheffler, M. & Ghiringhelli, L. M. Sisso: a compressed-sensing method for identifying the best low-dimensional descriptor in an immensity of offered candidates. *Phys. Rev. Mater.* **2**, 83802 (2018).
26. Sten, H. *et al.* The computational 2d materials database: high-throughput modeling and discovery of atomically thin crystals. *2D Mater.* **5**, 042002 (2018).
27. <https://cmr.fysik.dtu.dk/c2db/c2db.html>. Version of September 2020.
28. Gjerding, M. N. *et al.* Recent progress of the computational 2d materials database (c2db). *arXiv preprint arXiv:2102.03029* (2021).
29. Shen, Z.-X., Bo, X., Cao, K., Wan, X. & He, L. Magnetic ground state and electron-doping tuning of curie temperature in fe_3gete_2 : First-principles studies. *Phys. Rev. B* **103**, 85102 (2021).
30. Yamaguchi, M. & Hashimoto, T. Magnetic properties of cr_3te_4 in ferromagnetic region. *J. Phys. Soc. Jpn.* **32**, 635–638 (1972).
31. Goodenough, J. B. An interpretation of the magnetic properties of the perovskite-type mixed crystals $\text{la}_{1-x}\text{sr}_x\text{coo}_{3-\lambda}$. *J. Phys. Chem. Solids* **6**, 287–297 (1958).

32. Kanamori, J. Superexchange interaction and symmetry properties of electron orbitals. *J. Phys. Chem. Solids* **10**, 87–98 (1959).
33. Su, C. *et al.* Construction of crystal structure prototype database: methods and applications. *J. Phys. Condens. Matter* **29**, 165901–165901 (2017).
34. Lee, Y., Kotani, T. & Ke, L. Role of nonlocality in exchange correlation for magnetic two-dimensional van der waals materials. *Phys. Rev. B* **101**, 241409 (2020).
35. Menichetti, G., Calandra, M. & Polini, M. Electronic structure and magnetic properties of few-layer cr₂ge₂te₆: the key role of nonlocal electron–electron interaction effects. *2D Mater.* **6**, 045042 (2019).
36. Ke, L. & Katsnelson, M. I. Electron correlation effects on exchange interactions and spin excitations in 2d van der waals materials. *npj Comput. Mater.* **7**, 4 (2021).
37. Wu, M., Li, Z., Cao, T. & Louie, S. G. Physical origin of giant excitonic and magneto-optical responses in two-dimensional ferromagnetic insulators. *Nat. Commun.* **10**, 2371 (2019).
38. Wang, Y. *et al.* An effective structure prediction method for layered materials based on 2d particle swarm optimization algorithm. *J. Chem. Phys.* **137**, 224108 (2012).
39. Sharan, A. & Singh, N. Intrinsic valley polarization in computationally discovered two-dimensional ferrovalley materials: Lai₂ and pri₂ monolayers. *Adv. Theory Simul.* **5**, 2100476 (2022).
40. Blaha, P., Schwarz, K., Madsen, G., Kvasnicka, D. & Luitz, J. Wien2k: An augmented plane wave plus local orbitals program for calculating crystal properties. *Tech. Universitat Wien, Austria* **28** (2001).
41. Perdew, J. P., Burke, K. & Ernzerhof, M. Generalized gradient approximation made simple. *Phys. Rev. Lett.* **77**, 3865 (1996).
42. Torelli, D., Thygesen, K. S. & Olsen, T. High throughput computational screening for 2d ferromagnetic materials: the critical role of anisotropy and local correlations. *2D Mater.* **6**, 45018 (2019).
43. Wan, X., Dong, J. & Savrasov, S. Y. Mechanism of magnetic exchange interactions in europium monochalcogenides. *Phys. Rev. B* **83**, 205201 (2011).
44. Wang, D., Bo, X., Tang, F. & Wan, X. Calculated magnetic exchange interactions in the dirac magnon material cu₃teo₆. *Phys. Rev. B* **99**, 035160 (2019).

45. Bo, X., Wang, D., Wan, B. & Wan, X. Calculated magnetic exchange interactions in the quantum spin chain materials $\text{K}_2\text{CuSO}_4\text{Cl}_2$ and $\text{K}_2\text{CuSO}_4\text{Br}_2$. *Phys. Rev. B* **101**, 024416 (2020).
46. Swendsen, R. H. & Wang, J.-S. Replica monte carlo simulation of spin-glasses. *Phys. Rev. Lett.* **57**, 2607–2609 (1986).
47. Bruno, P. Absence of spontaneous magnetic order at nonzero temperature in one- and two-dimensional heisenberg and XY systems with long-range interactions. *Phys. Rev. Lett.* **87**, 137203 (2001).

Table 1. The structural prototypes of the 2DFM materials, and the chemical formula, space group of each compound. The calculated T_C (in K) and local magnetic moment (in μ_B per spin) are also shown. 1 L, 2 L, 3 L, and 4L denote that the 2DFM materials have 1, 2, 3, and 4 layers of magnetic atoms, respectively.

| Prototype | Chemical formula | Space group | T_C | M | Chemical formula | Space group | T_C | M |
|--|--|---------------|-------|-----|---|---------------|-------|-----|
| FeI ₂ -Fe (1 L) | CrO ₂ | <i>P-3m1</i> | 227 | 2.0 | FeCl ₂ | <i>P-6m2</i> | 199 | 4.0 |
| | FeBr ₂ | <i>P-6m2</i> | 148 | 4.0 | FeTe ₂ | <i>P-6m2</i> | 144 | 1.8 |
| | FeO ₂ | <i>P-3m1</i> | 107 | 2.0 | CrClI | <i>P3m1</i> | 101 | 4.0 |
| | FeI ₂ | <i>P-6m2</i> | 95 | 4.0 | CoO ₂ | <i>P-3m1</i> | 91 | 1.0 |
| | VSe ₂ | <i>P-6m2</i> | 78 | 1.0 | FeBr ₂ | <i>P-3m1</i> | 77 | 4.0 |
| | VS ₂ | <i>P-6m2</i> | 70 | 1.0 | VSSe | <i>P3m1</i> | 69 | 1.0 |
| | VTe ₂ | <i>P-6m2</i> | 60 | 1.0 | VSeTe | <i>P3m1</i> | 57 | 1.0 |
| | CrBrI | <i>P3m1</i> | 52 | 4.0 | RhI ₂ | <i>P-3m1</i> | 47 | 1.0 |
| | VSTe | <i>P3m1</i> | 37 | 1.1 | FeI ₂ | <i>P-3m1</i> | 26 | 4.0 |
| | ScCl ₂ | <i>P-6m2</i> | 19 | 1.0 | ScBr ₂ | <i>P-6m2</i> | 17 | 1.0 |
| | VS ₂ | <i>P-3m1</i> | 16 | 0.5 | ScI ₂ | <i>P-6m2</i> | 15 | 1.0 |
| | TmI ₂ | <i>P-3m1</i> | 14 | 0.9 | VSSe | <i>P3m1</i> | 12 | 0.7 |
| | NbSeTe | <i>P3m1</i> | 12 | 0.8 | NbSTe | <i>P3m1</i> | 10 | 0.7 |
| | NbTe ₂ | <i>P-6m2</i> | 8 | 0.9 | YBr ₂ | <i>P-6m2</i> | 3 | 1.0 |
| | YCl ₂ | <i>P-6m2</i> | 3 | 1.0 | | | | |
| CrI ₃ -Cr (1 L) | V ₂ Cl ₆ | <i>P-31m</i> | 60 | 2.0 | V ₂ Br ₆ | <i>P-31m</i> | 60 | 2.0 |
| | V ₂ I ₆ | <i>P-31m</i> | 60 | 2.0 | Ru ₂ Cl ₆ | <i>P-31m</i> | 58 | 1.0 |
| | Os ₂ Cl ₆ | <i>P-31m</i> | 56 | 1.0 | Ti ₂ Cl ₆ | <i>P-62m</i> | 42 | 1.0 |
| | Ti ₂ Br ₆ | <i>P-62m</i> | 40 | 1.0 | Re ₂ Br ₆ | <i>P-31m</i> | 40 | 2.0 |
| | Ru ₂ Br ₆ | <i>P-31m</i> | 30 | 1.0 | Ni ₂ I ₆ | <i>P-31m</i> | 26 | 1.0 |
| | CrI ₃ | <i>P-31m</i> | 26 | 3.0 | Ni ₂ Br ₆ | <i>P-31m</i> | 20 | 1.0 |
| | Os ₂ I ₆ | <i>P-31m</i> | 11 | 1.0 | Cr ₂ Ge ₂ Te ₆ | <i>P-31m</i> | 11 | 3.0 |
| VO ₂ -V (1 L) | Ni ₂ I ₂ | <i>P4/nmm</i> | 166 | 1.0 | VO ₂ | <i>P-4m2</i> | 152 | 1.0 |
| | Ni ₂ O ₂ | <i>P4/nmm</i> | 127 | 1.2 | Mn ₂ Se ₂ | <i>P4/nmm</i> | 104 | 1.4 |
| | Ni ₂ Se ₂ | <i>P4/nmm</i> | 103 | 0.6 | Mn ₂ S ₂ | <i>P4/nmm</i> | 87 | 1.3 |
| | Ni ₂ S ₂ | <i>P4/nmm</i> | 87 | 0.5 | Ni ₂ Te ₂ | <i>P4/nmm</i> | 83 | 0.6 |
| | CrI ₂ | <i>P-4m2</i> | 75 | 4.0 | Mn ₂ Te ₂ | <i>P4/nmm</i> | 65 | 1.5 |
| | Co ₂ S ₂ | <i>P4/nmm</i> | 59 | 0.5 | Cr ₂ Se ₂ | <i>P4/nmm</i> | 43 | 0.3 |
| | Cr ₂ S ₂ | <i>P4/nmm</i> | 41 | 0.4 | Rh ₂ S ₂ | <i>P4/nmm</i> | 35 | 0.3 |
| | NiBr ₂ | <i>P-4m2</i> | 29 | 2.0 | | | | |
| Co ₂ F ₂ -Co (2 L) | Co ₂ F ₂ | <i>P-3m1</i> | 542 | 2.4 | Ni ₂ I ₂ | <i>P-3m1</i> | 137 | 1.0 |
| | ErHCl | <i>P-3m1</i> | 61 | 2.6 | YbOCl | <i>P-3m1</i> | 33 | 1.0 |
| | Sc ₂ Cl ₂ | <i>P-3m1</i> | 11 | 0.8 | Sc ₂ Br ₂ | <i>P-3m1</i> | 11 | 0.8 |
| Cr ₂ I ₂ S ₂ -Cr (2 L) | Mn ₂ I ₂ O ₂ | <i>Pmmm</i> | 127 | 4.0 | Mn ₂ I ₂ N ₂ | <i>Pmmm</i> | 117 | 3.0 |
| | V ₂ Br ₂ O ₂ | <i>Pmmm</i> | 98 | 2.0 | Mn ₂ Cl ₂ N ₂ | <i>Pmmm</i> | 93 | 3.0 |
| | Cr ₂ I ₂ Se ₂ | <i>Pmmm</i> | 90 | 3.0 | Cr ₂ I ₂ S ₂ | <i>Pmmm</i> | 88 | 3.0 |
| | Cr ₂ Br ₂ S ₂ | <i>Pmmm</i> | 81 | 3.0 | Cr ₂ Cl ₂ S ₂ | <i>Pmmm</i> | 66 | 3.0 |
| | HoSI | <i>Pmmm</i> | 30 | 4.0 | | | | |
| Zr ₂ I ₂ S ₂ -Zr (1 L) | Zr ₂ I ₂ S ₂ | <i>Pc</i> | 5 | 0.8 | | | | |
| EuOI-Eu (2 L) | EuOI | <i>P4/nmm</i> | 35 | 7.4 | | | | |
| V ₃ N ₂ O ₂ -V (3 L) | V ₃ N ₂ O ₂ | <i>P-6m2</i> | 71 | 1.0 | | | | |
| Cr ₃ Te ₄ -Cr 3 L | Cr ₃ Te ₄ | <i>P-3m1</i> | 133 | 3.3 | | | | |
| Fe ₃ GeTe ₂ -Fe (3 L) | Fe ₃ GeTe ₂ | <i>P-6m2</i> | 158 | 1.5 | | | | |
| Fe ₄ GeTe ₂ -Fe (4 L) | Fe ₄ GeTe ₂ | <i>P-3m1</i> | 207 | 2.1 | | | | |